JOURNAL OF GUIDANCE, CONTROL, AND DYNAMICS
Vol. 20, No. 3, May–June 1997

Planar Aeroassisted Attainability Domain

M. Guelman*
Technion—Israel Institute of Technology, Haifa 32000, Israel

The purpose is to study the general problem of aerodynamic maneuvers at low altitudes while at orbital speed. The spacecraft's trajectory changes are generated by the applied lift and drag aerodynamic forces. Employing an adequate model of the aerodynamic forces function of the angle of attack, the unbounded angle of attack is used as the control variable. To perform a general analysis of spacecraft trajectories when employing aerodynamic forces, the aeroassisted attainability domain is studied. Specifically, given the initial position and velocity of the vehicle at atmospheric entry, the region in state space that can be attained by the vehicle at atmospheric exit when using all of the possible controls at its disposal is determined. The set of trajectories belonging to the boundary of the attainability domain is obtained through the variation of a single parameter, namely, the initial value of angle of attack at atmospheric entry. The trajectories are obtained by a forward integration of the state and adjoint equations of motion. Representative results of the attainability domain for given initial conditions and vehicle characteristics are presented.

Nomenclature

C_D = drag coefficient
C_L = lift coefficient
C_N = normal force coefficient
C_T = tangential force coefficient
D = drag force
F_N = aerodynamic normal force
F_T = aerodynamic tangential force
g = gravity acceleration
H = Hamiltonian
h = density scale height
L = lift force
m = spacecraft mass
R = radial distance from the center of the Earth
R_e = Earth radius
r = normalized distance
S = reference surface
V = spacecraft velocity
v = normalized spacecraft velocity
α = angle of attack
β = density inverse scale height
γ = flight-path angle
θ = rotation angle
λ_r = range adjoint
λ_v = velocity adjoint
λ_γ = flight-path angle adjoint
μ = Earth gravitational constant
ρ = atmosphere density
σ = normalized retrograde time
υ = normalized forward time
ω_e = orbital frequency

Introduction

THE possibility of using aerodynamic forces to change orbital altitude and/or inclination with an energy expenditure smaller than that associated with an exoatmospheric propulsive maneuver has been considered since the early 1960s (Ref. 1). Some of the missions where aeroassisted maneuvers can provide a significant reduction in fuel expenditure include transfer of a payload from geosynchronous orbit to rendezvous with either a Shuttle or space station,[2] orbital insertion around the planet Mars,[3] and change of the orbital inclination.[4] Two comprehensive survey papers[5,6] were published during the 1980s on aeroassisted transfer.

In the past, approximate optimal aeroassisted maneuvers were developed by solving calculus of variations nonlinear, two-point boundary value problems from a particular starting state of the system to a desired final state. Fuel minimization was achieved by adequately defining the required initial conditions at atmospheric entry, as obtained from an exoatmospheric maneuver, and then again by adequately defining the aeroassited maneuver final conditions at atmospheric exit, such that the required fuel for final orbit insertion be a minimum.

In an aeroassisted maneuver the spacecraft orbital changes are due to the applied lift and drag aerodynamic forces. Generally, the aerodynamic forces were modeled using a standard polar drag model relating drag to lift and employing lift as the control variable. However, it is the angle of attack that the spacecraft attitude control system is able to directly control. Employing an adequate model of the aerodynamic forces as a function of the angle of attack, the angle of attack can be directly employed as the control variable.

To perform a general analysis of the spacecraft trajectories when employing aerodynamic forces, the planar aeroassisted attainability domain is studied. Specifically, given the initial position and velocity of the vehicle at atmospheric entry, the region in state space that can be reached by the vehicle at atmospheric exit is determined, when using all of the possible controls at its disposal.

The attainable domain from a certain state is equivalent to the controllability domain to the same state, depending on the sense of time,[7] i.e., the set of trajectories to final points that can be attained from a certain state is the same as the set of trajectories from the points controllable to the same state, with the trajectories traversed in the retrograde sense. A basic theorem on controllability is employed to determine the trajectories belonging to the boundary of the attainability domain. These trajectories are obtained by a forward integration of the equations of motion as well as of the adjoint variables. The set of trajectories defining the attainability domain boundary is obtained through the variation of a single parameter, namely, the initial angle of attack at atmospheric entry.

System Model

Figure 1 depicts the spacecraft in the central gravitational field of the Earth, under the influence of both aerodynamic and gravitational forces, where γ is the flight-path angle with respect to the local horizon. The vehicle is able to control its attitude and, thus, its angle-of-attack α.

The aerodynamic normal and tangential forces in body axes are defined by

$$F_N = \tfrac{1}{2}\rho V^2 S C_N \sin\alpha \tag{1}$$

$$F_T = \tfrac{1}{2}\rho V^2 S C_T \cos\alpha \tag{2}$$

Received June 10, 1996; presented as Paper 96-3595 at the AIAA/AAS Astrodynamics Specialist Conference, San Diego, CA, July 29–31, 1996; revision received Feb. 7, 1997; accepted for publication Feb. 10, 1997.

*Professor, Faculty of Aerospace Engineering. Member AIAA.

where C_N and C_T are the aerodynamic normal and tangential coefficients assumed to be constant and ρ is the air mass density, an exponential function of the flight altitude

$$\rho = \rho_0 \exp\{-[(R - R_0)/h]\} \tag{3}$$

where ρ_0 is the atmospheric density at a reference altitude R_0 and h is the altitude scale factor.

This particular simple model for the aerodynamic forces, as defined by expressions (1) and (2), closely approximates the model generally employed for small angles of attack. For large angles of attack it represents a fairly valid model: 1) the normal force slope decreases with increasing angle of attack and the force amplitude is symmetric with respect to $\alpha = \pi/2$, 2) the tangential force is null for $\alpha = \pi/2$ and changes sign for $\alpha > \pi/2$, and 3) the drag and lift coefficients C_D and C_L agree fairly well with the coefficients obtained from the Newtonian theory of flow. Effectively, projecting the normal and tangential forces along, and normal to, the velocity vector and after performing adequate trigonometric manipulations, the drag and lift forces are

$$D = \tfrac{1}{2}\rho V^2 S C_D \tag{4}$$

$$L = \tfrac{1}{2}\rho V^2 S C_L \tag{5}$$

where

$$C_D = \tfrac{1}{2}(C_N - C_T)(k - \cos 2\alpha) \tag{6}$$

$$C_L = \tfrac{1}{2}(C_N - C_T)\sin 2\alpha \tag{7}$$

with

$$k = \frac{C_N + C_T}{C_N - C_T} > 1 \tag{8}$$

Figure 2 shows the drag and lift coefficients of a flat plate as a function of the angle of attack, both, according to Newtonian theory of flow past bodies with specular reflection of molecules,[8] as well as the approximated model coefficients. As can be clearly seen, the drag and lift coefficients agree fairly well with the coefficients obtained from the Newtonian flow theory. The approximate model includes, in addition, combined form and friction effects generating a nonzero drag coefficient at zero angle of attack.

In conclusion then, the aerodynamic forces, as defined by expressions (1) and (2), are a valid model both for low and high angles of attack.

This specific model of the aerodynamic coefficients corresponds, in terms of conventional aerodynamic representation, to a circular polar drag. Coefficients C_N, C_T, and k can be defined such that they provide a close approximation to the original parabolic polar drag. Figure 3 shows the parabolic, circular, and elliptic polar[9] drags for the case studied in Ref. 10. Unlike the parabolic polar drag, the circular, as well as the elliptic polar drag, has a maximum lift coefficient and, hence, provides a better approximation to actual polar drag at high angles of attack.

The system equations of motion are defined by

$$\dot{V} = -(D/m) - g\sin\gamma \tag{9}$$

$$V\dot{\gamma} = (L/m) - g\cos\gamma + (V^2/R)\cos\gamma \tag{10}$$

$$R\dot{\theta} = V\cos\gamma \tag{11}$$

$$\dot{R} = V\sin\gamma \tag{12}$$

where $g = \mu/R^2$.

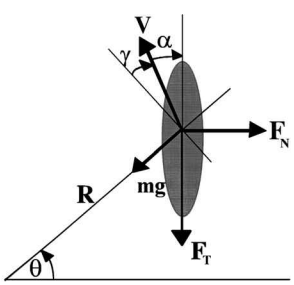

Fig. 1 Spacecraft gravitational and aerodynamic forces.

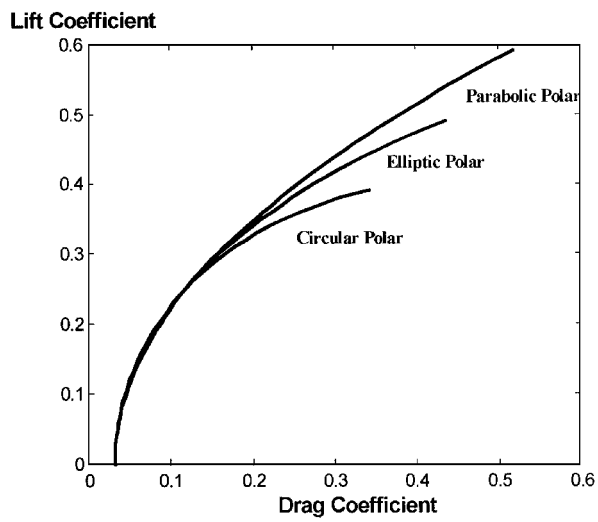

Fig. 3 Parabollic, elliptic, and circular polar drags.

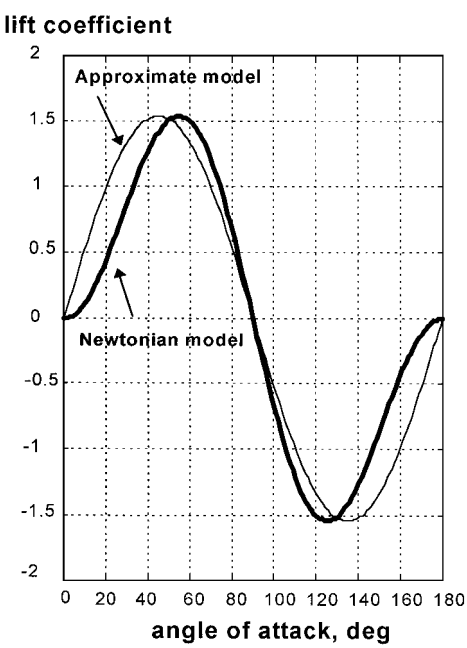

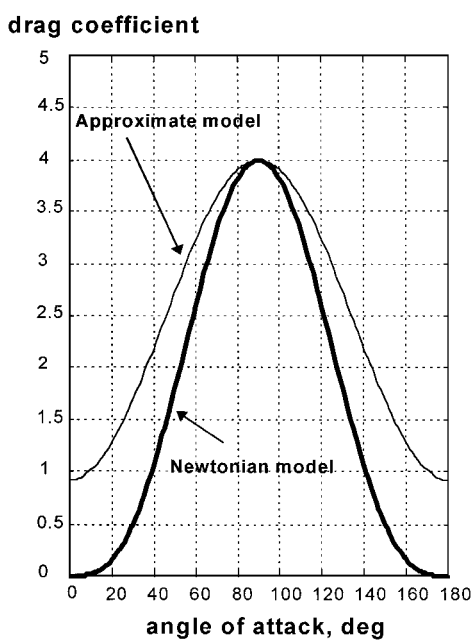

Fig. 2 Newtonian and approximated drag and lift coefficients.

Let us define the normalized variables as follows:

$$r = R/R_e \tag{13}$$

$$v = V/R_e\omega_e \tag{14}$$

$$\upsilon = \omega_e t \tag{15}$$

where

$$\omega_e = \left(\mu/R_e^3\right)^{\frac{1}{2}} \tag{16}$$

Changing variables, the following system in normalized coordinates is obtained:

$$\dot{\theta} = v\cos\gamma/r \tag{17}$$

$$\dot{r} = v\sin\gamma \tag{18}$$

$$\dot{v} = c_1\rho_n(r)(\cos 2\alpha - k)v^2 - (\sin\gamma/r^2) \tag{19}$$

$$\dot{\gamma} = c_1\rho_n(r)v\sin 2\alpha - \frac{\cos\gamma}{r^2 v} + \frac{v\cos\gamma}{r} \tag{20}$$

where the dot now indicates the derivative with respect to υ. Furthermore,

$$c_1 = \frac{1}{4}\frac{S(C_N - C_T)\rho_0}{m}R_e \tag{21}$$

and $\rho_n = \exp\{-\beta(r - r_0)\}$ with $\beta = R_e/H$.

It is seen that the system equations are independent of θ, i.e., θ is an ignorable variable.

Controllability Minimum Principle

The problem to be solved is to find the boundaries of the attainability set for a vehicle entering the atmosphere at r_0 with velocity v_0 and flight path direction γ_0. For this purpose, we shall employ the method presented in Ref. 11.

Depending on the sense of time, the attainability domain from a certain state is equivalent to the controllability domain to the same state.[7] Based on this equivalence, the attainability domain boundary can be obtained solving the controllability problem.

Under the assumption that the controllability set is closed, it is shown that system paths exist to the target state from every point on the boundary of the controllable set. These paths remain entirely on the boundary of the controllable set Ξ. This is a particular case of the more general concept of barriers of a game, where control is exercised by two opposing players. The necessary conditions for determining the controls of the paths on Ξ appear in the following controllability minimum principle.[12]

Let $\boldsymbol{u}^*$ be an admissible control, which generates a solution $\boldsymbol{x}^* : [t_0, t_1] \to \Xi$ to the state equations $\dot{\boldsymbol{x}} = \boldsymbol{f}(\boldsymbol{x}, \boldsymbol{u})$, $\boldsymbol{u} \in \Omega$, such that $\boldsymbol{x}^*(t) \in \Xi$, for all $t \in [t_0, t_1]$.

Then, with $\boldsymbol{\lambda} = (\lambda_1, \ldots, \lambda_n)$ and

$$H(\boldsymbol{\lambda}, \boldsymbol{x}, \boldsymbol{u}) = \boldsymbol{\lambda}^T \boldsymbol{f}(\boldsymbol{x}, \boldsymbol{u})$$

there exists a nonzero continuous solution $\boldsymbol{\lambda} : [t_0, t_1] \to E^n$ to the adjoint equations:

$$\dot{\boldsymbol{\lambda}} = -\frac{\partial H(\boldsymbol{\lambda}, \boldsymbol{x}^*, \boldsymbol{u}^*)}{\partial \boldsymbol{x}}$$

such that

$$H(\boldsymbol{\lambda}, \boldsymbol{x}^*, \boldsymbol{u}^*) = \min_{\boldsymbol{u}\in\Omega} H(\boldsymbol{\lambda}, \boldsymbol{x}, \boldsymbol{u}) = 0 \qquad \forall t \in [t_0, t_1]$$

Furthermore, if the terminal point $\boldsymbol{x}^*(t_1)$ is a regular interior point of the limiting surface Ξ, then the terminal transversality condition is satisfied.

Boundary Trajectories

To find the boundary trajectories of the attainability domain from state r_0, v_0, and γ_0, the equivalent controllability problem to terminal state r_0, v_0, and γ_0 will be solved. For this purpose, υ is changed into $\sigma = -\upsilon$, and the system equations become

$$\mathring{r} = -v\sin\gamma \tag{22}$$

$$\mathring{v} = -c_1\rho_n(\cos 2\alpha - k)v^2 + (\sin\gamma/r^2) \tag{23}$$

$$\mathring{\gamma} = -c_1\rho_n v\sin 2\alpha + \frac{\cos\gamma}{r^2 v} - \frac{v\cos\gamma}{r} \tag{24}$$

where $\circ$ is the derivative with respect to σ.

Let us write the Hamiltonian of the system (22–24):

$$H = -\lambda_r v\sin\gamma - \lambda_v\left[c_1\rho_n v^2(\cos 2\alpha - k) - \frac{\sin\gamma}{r^2}\right] - \lambda_\gamma\left(c_1\rho_n v\sin 2\alpha - \frac{\cos\gamma}{r^2 v} + \frac{v\cos\gamma}{r}\right) \tag{25}$$

with adjoint vectors,

$$\mathring{\lambda}_r = -\frac{\partial H}{\partial r} = \lambda_v\left[c_1 v^2(\cos 2\alpha - k)\frac{\mathrm{d}\rho_n}{\mathrm{d}t} + \frac{2\sin\gamma}{r^3}\right] + \lambda_\gamma\left[c_1 v\sin 2\alpha\frac{\mathrm{d}\rho_n}{\mathrm{d}t} + \frac{2\cos\gamma}{vr^3} - \frac{v\cos\gamma}{r^2}\right] \tag{26}$$

$$\mathring{\lambda}_v = -\frac{\partial H}{\partial v} = \lambda_r\sin\gamma + \lambda_v c_1\rho_n 2v(\cos 2\alpha - k) + \lambda_\gamma\left[c_1\rho_n\sin 2\alpha + \frac{\cos\gamma}{v^2 r^2} + \frac{\cos\gamma}{r}\right] \tag{27}$$

$$\mathring{\lambda}_\gamma = -\frac{\partial H}{\partial \gamma} = \lambda_r v\cos\gamma - \frac{\lambda_v\cos\gamma}{r^2} + \lambda_\gamma\left[\frac{\sin\gamma}{vr^2} - \frac{v\sin\gamma}{r}\right] \tag{28}$$

and from the transversality conditions, λ_{r0}, λ_{v0}, and $\lambda_{\gamma 0}$ are free.

To minimize the Hamiltonian, it is found that

$$\sin 2\alpha^* = \frac{\lambda_\gamma}{\sqrt{\lambda_\gamma^2 + (v\lambda_v)^2}} \tag{29}$$

$$\cos 2\alpha^* = \frac{v\lambda_v}{\sqrt{\lambda_\gamma^2 + (v\lambda_v)^2}} \tag{30}$$

We shall now show that the system of adjoint equations can be reduced to a single equation. For this purpose let us define new variables

$$\lambda\cos\varphi = v\lambda_v \tag{31}$$

$$\lambda\sin\varphi = \lambda_\gamma \tag{32}$$

Differentiating Eqs. (31) and (32) with respect to σ and solving for $\mathring{\lambda}$ and $\mathring{\varphi}$,

$$\mathring{\lambda} = (v\mathring{\lambda}_v)\cos\varphi + \mathring{\lambda}_\gamma\sin\varphi \tag{33}$$

$$\mathring{\varphi} = \frac{-(v\mathring{\lambda}_v)\sin\varphi + \mathring{\lambda}_\gamma\cos\varphi}{\lambda} \tag{34}$$

Introducing Eqs. (31) and (32) into Eqs. (29) and (30),

$$\sin 2\alpha^* = \sin\varphi \tag{35}$$

$$\cos 2\alpha^* = \cos\varphi \tag{36}$$

that is, $\varphi = 2\alpha^*$.

Introducing Eqs. (31), (32), (35), and (36) into Eqs. (25), (27), and (28) and rearranging,

$$H^* = -\lambda_r v \sin\gamma - \lambda\left[c_1\rho v(1-k\cos\varphi) - \frac{\sin(\gamma+\varphi)}{vr^2} + \frac{v\cos\gamma\sin\varphi}{r}\right] = 0 \tag{37}$$

$$\mathring{\lambda}_v = \lambda_r \sin\gamma + c_1\rho_n\lambda(1-2k\cos\varphi+\cos^2\varphi) + \lambda\sin\varphi\cos\gamma[(1/v^2r^2)+(1/v)] \tag{38}$$

$$\mathring{\lambda}_\gamma = \lambda_r v\cos\gamma - \lambda\left[\frac{\cos(\varphi+\gamma)}{vr^2} + \frac{v\sin\varphi\sin\gamma}{r}\right] \tag{39}$$

Rearranging Eq. (37),

$$\lambda_r = -\frac{\lambda}{v\sin\gamma}\left[c_1\rho_n v(1-k\cos\varphi) - \frac{\sin(\gamma+\varphi)}{vr^2} + \frac{v\cos\gamma\sin\varphi}{r}\right] \tag{40}$$

Introducing Eq. (40) into Eqs. (38) and (39) and rearranging,

$$\mathring{\lambda}_v = c_1\rho_n(\cos\varphi - k)\lambda\cos\varphi + (\lambda/v^2r^2) \times [\sin(\gamma+\varphi)+\sin\varphi\cos\gamma] \tag{41}$$

$$\mathring{\lambda}_\gamma = -\frac{\lambda}{\sin\gamma}\left[c_1\rho_n v(1-k\cos\varphi)\cos\gamma - \frac{\sin\varphi}{vr^2} + \frac{v\sin\varphi}{r}\right] \tag{42}$$

Now, multiplying Eq. (41) by v, adding to Eq. (23) multiplied by λ_v, and rearranging,

$$(v\mathring{\lambda}_v) = \frac{2\lambda\sin(\gamma+\varphi)}{vr^2} \tag{43}$$

Introducing Eqs. (42) and (43) into Eq. (34) and rearranging,

$$\mathring{\varphi} = -\frac{1}{\sin\gamma}\left[c_1\rho_n v(1-k\cos\varphi)\cos\varphi\cos\gamma - \frac{\sin\varphi[2\sin\gamma\sin(\gamma+\varphi)+\cos\varphi]}{vr^2} + \frac{v\sin\varphi\cos\varphi}{r}\right] \tag{44}$$

We have finally reduced the system of adjoint equations to this single equation defining φ, and consequently α^*, along a boundary trajectory.

Attainability Domain

The solution of the controllability domain problem to state r_0, v_0, and γ_0 is obtained by solving backward in time Eqs. (22–24) and (44) from final conditions r_0, v_0, γ_0, and φ_0. Equivalently, the solution of the attainability domain problem from state r_0, v_0, and γ_0 is obtained by solving forward in time the following equations:

$$\dot{r} = v\sin\gamma \tag{45}$$

$$\dot{v} = c_1\rho_n(\cos\varphi - k)v^2 - (\sin\gamma/r^2) \tag{46}$$

$$\dot{\gamma} = c_1\rho_n v\sin\varphi - \frac{\cos\gamma}{r^2v} + \frac{v\cos\gamma}{r} \tag{47}$$

$$\dot{\varphi} = \frac{1}{\sin\gamma}\left[c_1\rho_n v(1-k\cos\varphi)\cos\varphi\cos\gamma - \frac{\sin\varphi[2\sin\gamma\sin(\gamma+\varphi)+\cos\varphi]}{vr^2} + \frac{v\sin\varphi\cos\varphi}{r}\right] \tag{48}$$

from initial conditions r_0, v_0, γ_0, and φ_0. Here φ_0 is the parameter generating the set of trajectories defining the boundary surface of the controllability (attainability) domain. Because $\alpha^* = \frac{1}{2}\varphi$, the parameter is effectively the initial angle of attack at atmospheric entry.

For given initial values of velocity and flight-path angle at atmospheric entry, the intersection of the attainability domain with the atmospheric boundary defines the attainable values of velocity and flight-path angle at atmospheric exit. These values of velocity and flight-path angle are the initial conditions for the exoatmospheric orbit in an aeroassisted transfer.

Numerical Results

The physical constants employed for the numerical computations are given in Table 1, and the spacecraft characteristics are given in Table 2. The vehicle characteristics approximate those of the vehicle in Ref. 10 with the same zero lift drag and a maximum lift to drag ratio $E^* = 2.3$.

From a numerical standpoint it is to be remarked that, for $\gamma = 0$, both the numerator and denominator in Eq. (44) become zero. To avoid singularities in the numerical computation, the adjoint equations obtained from Eqs. (22), (24), and (32) with time in the forward direction are solved to obtain adjoint variables λ_r, λ_γ, and $v\lambda_v$ with initial conditions:

$$(v\lambda_v)_0 = \cos\varphi_0 \tag{49}$$

$$\lambda_{\gamma 0} = \sin\varphi_0 \tag{50}$$

and from the Hamiltonian given in Eq. (25),

$$\lambda_{r0} = -\frac{1}{v_0\sin\gamma_0}\left[c_1\rho_n(r_0)v_0(1-k\cos\varphi_0) - \frac{\sin(\gamma_0+\varphi_0)}{v_0r_0^2} + \frac{v_0\cos\gamma_0\sin\varphi_0}{r_0}\right] \tag{51}$$

This set of equations is solved together with Eqs. (45–47), where $\varphi = 2\alpha^*$ is obtained from Eqs. (29) and (30). The solution of this set of equations with initial parameter φ_0 such that $-\pi \le \varphi_0 \le \pi$ will generate the boundary of the attainability domain.

Two different cases will be presented for the same vehicle depending on the initial conditions at atmospheric entry. Initial conditions for cases 1 and 2 are given in Tables 3 and 4, respectively. Case 1

Table 1 Physical constants

Earth radius r_e	6378 km
Earth gravity constant μ	3.99×10^5 km^3/s^2
Altitude density reference h_0	36.5 km
Reference altitude density ρ_0	6.9×10^6 kg/km^3
Scale height H	7.62 km

Table 2 Vehicle characteristics

Mass to area ratio m/S	300 kg/m^2
Zero lift drag coefficient C_{D0}	$C_T = 0.1$
Normal force coefficient C_N	1.1

Table 3 Case 1, hyperbolic entry

Atmosphere entry altitude h_T	120 km
Flight-path angle γ_0	−5 deg
Entry velocity V_0	12 km · s^{-1}

Table 4 Case 2, elliptic entry

Atmosphere entry altitude h_T	120 km
Flight-path angle γ_0	−4.5 deg
Entry velocity V_0	10.15 km · s^{-1}

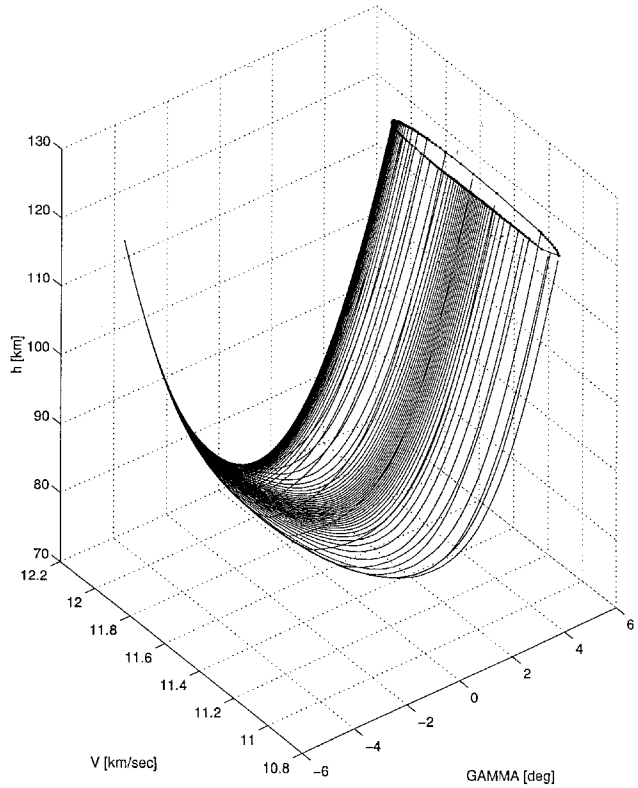

Fig. 4 Attainability domain in three-dimensional space V, h, and γ for case 1.

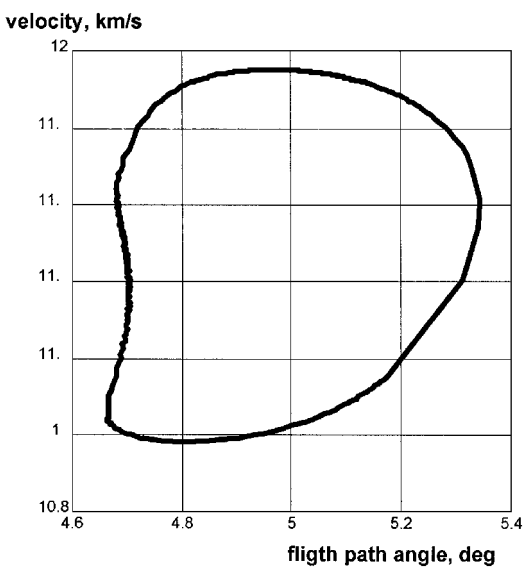

Fig. 5 Attainability domain intersection with the atmosphere boundary.

corresponds to entry into the atmosphere at hyperbolic velocity with respect to Earth. Case 2 corresponds to elliptic velocity with respect to Earth. Figure 4 shows the attainability domain boundary for hyperbolic atmosphere entry in the three-dimensional space defined by altitude, velocity, and flight-path angle. In this case, as can be clearly seen, all of the trajectories exit the atmosphere.

Figure 5 shows the intersection of the attainability domain with the atmosphere boundary ($h_T = 120$ km). From this map of velocity and flight-path angle, the flight paths with extreme velocity values can readily be obtained.

In Fig. 6 is shown the attainability domain boundary for elliptic atmosphere entry in the three-dimensional space defined by altitude, velocity, and flight-path angle. For the case of elliptic velocity

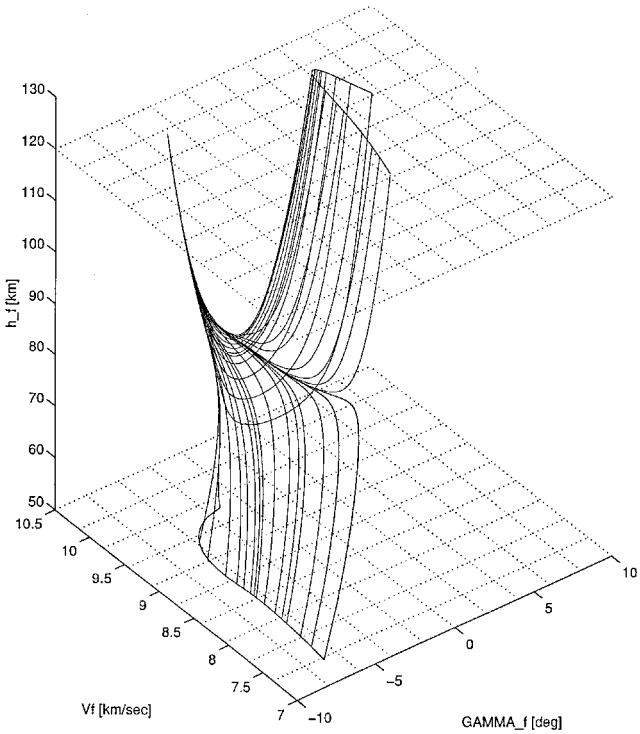

Fig. 6 Attainability domain in three-dimensional space V, h, and γ for case 2.

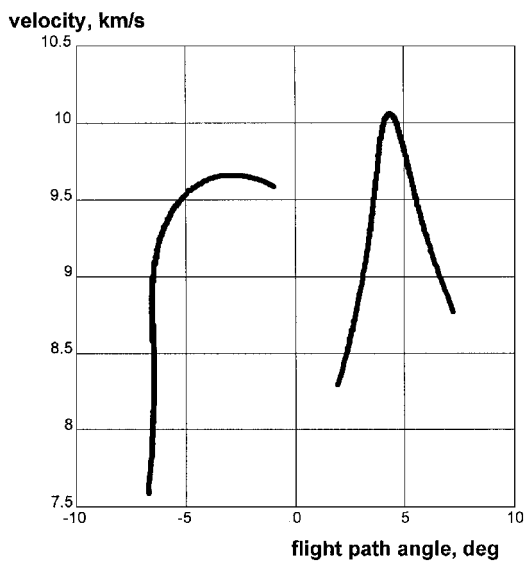

Fig. 7 Velocity vs flight-path angle for exiting and entering trajectories.

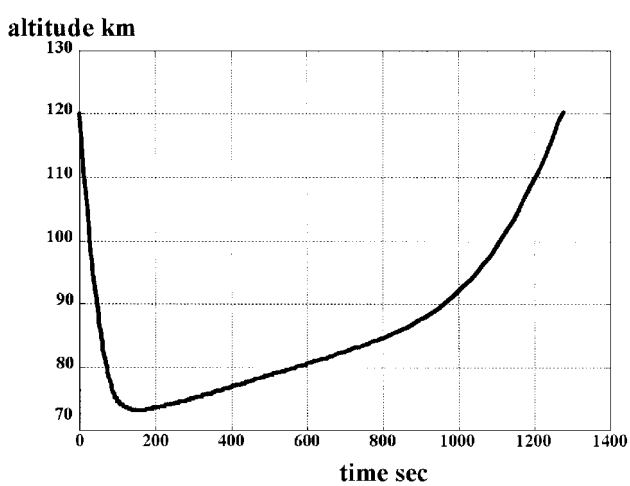

Fig. 8 Altitude vs time for the limiting exit boundary trajectory.

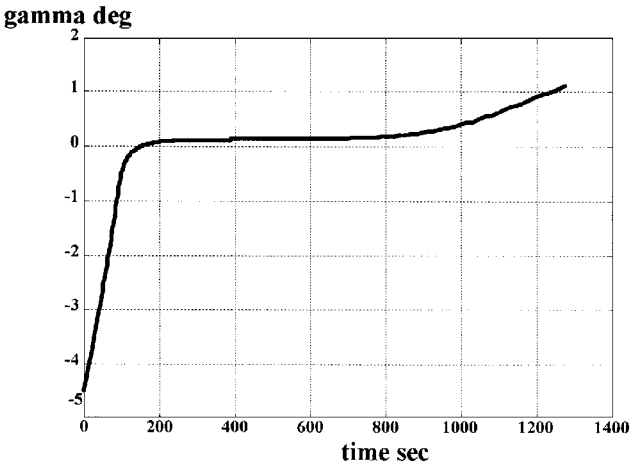

Fig. 9 Flight-path angle vs time for the limiting exit boundary trajectory.

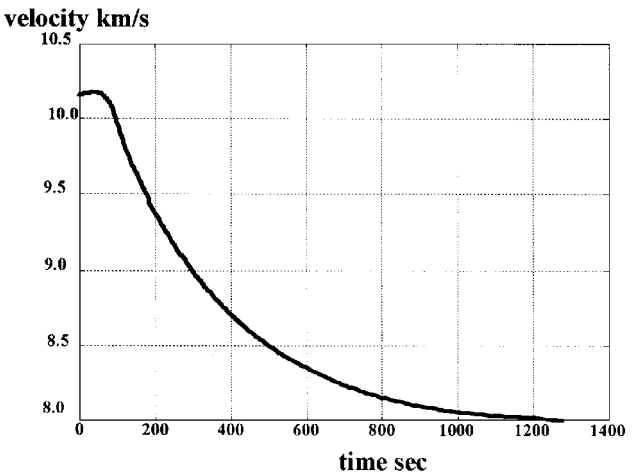

Fig. 10 Velocity vs time for the limiting exit boundary trajectory.

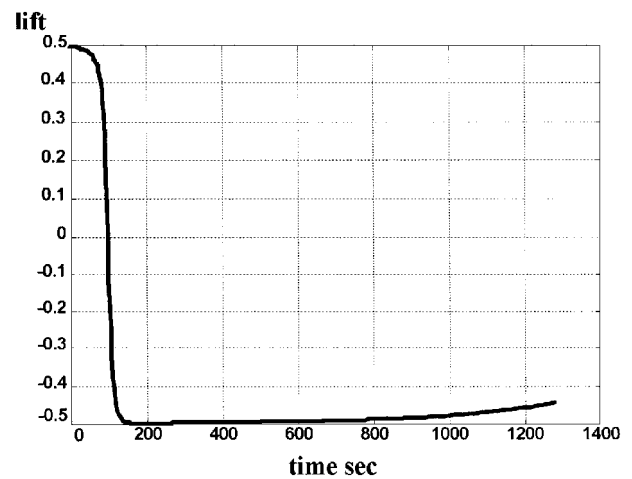

Fig. 11 Lift control vs time for the limiting exit trajectory.

entry, there are two sets of trajectories, those exiting the atmosphere boundary and those descending toward the Earth's surface.

Figure 7 shows the velocity vs flight-path angle corresponding to either the intersection of the attainability domain exiting boundary trajectories with the atmospheric boundary or the attainability domain entering boundary trajectories crossing the 50-km altitude level. Those trajectories exiting the atmospheric boundary have a positive flight-path angle and those crossing the 50-km altitude level have a negative flight-path angle, finally reaching the Earth's surface. The limiting exit trajectory separating the exiting and entering trajectories is of particular interest. Altitude, flight-path angle, and velocity of this limiting trajectory are all shown as functions of time in Figs. 8, 9, and 10, respectively. These boundary trajectories have the same characteristics as the optimal trajectories of Ref. 10. They have three branches, a relatively short descending branch, a very short nearly horizontal flight branch ($\gamma \approx 0$), and a long ascending flight branch.

The lift control for the limiting exit trajectory is shown in Fig. 11. After an initial positive lift most of the trajectory is flown with maximum negative lift coefficient ($\alpha^* \approx -45$ deg).

Conclusions

Based on a simple but realistic model of the aerodynamic forces acting on a spacecraft entering Earth's atmosphere at orbital speed, the set of trajectories belonging to the boundary of the attainability domain is obtained through the variation of a single parameter, namely, the initial value of angle of attack at atmospheric entry. The trajectories are obtained by a forward integration of the state and adjoint equations of motion. If final conditions for transfer can be achieved with the boundary trajectories, these trajectories can be generated without recourse to solving the difficult two point boundary value problem as is generally the case.

The determination of the attainability domain provides a global view of the vehicle's performance. The attainability domain for given initial entry conditions clearly depends on the vehicle's aerodynamic characteristics. Because of the relative simplicity of the approach presented here for the determination of the attainability domain, its analysis as a function of the aerodynamic parameters can be performed to define desired vehicle characteristics.

Acknowledgment

This work was supported by the Jack Adler Foundation under Grant 165-023-95 administered by the Israel Academy of Sciences and Humanities.

References

[1]London, H. S., "Change of Satellite Orbit Plane by Aerodynamic Maneuvering," *Journal of the Aerospace Sciences*, Vol. 29, March 1962, pp. 323–332.

[2]Anon., "Orbit Transfer Systems with Emphasis on Shuttle Applications—1986–1991," NASA TM X-73394, April 1977.

[3]Wetzel, T. A., and Moerder, D. D., "Vehicle/Trajectory Optimization for Aerocapture at Mars," *Journal of the Astronautical Sciences*, Vol. 42, No. 1, 1994, pp. 71–89.

[4]Mease, K. D., Vinh, N. X., and Kuo, S. H., "Optimal Plane Change During Constant Altitude Hypersonic Flight," *Journal of Guidance, Control, and Dynamics*, Vol. 14, No. 4, 1991, pp. 797–806.

[5]Walberg, G. D., "A Survey of Aeroassisted Orbit Transfer," *Journal of Spacecraft and Rockets*, Vol. 22, No. 1, 1985, pp. 3–18.

[6]Mease, K. D., "Optimization of Aeroassisted Orbit Transfer; Current Status," *Journal of the Astronautical Sciences*, Vol. 36, Nos. 1/2, 1988, pp. 7–33.

[7]Snow, D. R., "Determining Reachable Regions and Optimal Controls," *Advances in Control Systems*, Vol. 5, edited by C. T. Leondes, Academic, New York, 1967, pp. 133–195.

[8]Shidlovskiy, V. P., *Introduction to Dynamics of Rarefied Gases*, Elsevier, New York, 1967, pp. 32–37.

[9]Hull, D. G., McClendon, J. R., and Speyer, J. L., "Aeroassisted Orbital Plane Change Using an Elliptic Drag Polar," *Journal of the Astronautical Sciences*, Vol. 36, Nos. 1/2, 1988, pp. 73–87.

[10]Miele, A., Wang, T., and Lee, W. Y., "Optimization and Guidance of Trajectories for Coplanar Aeroassisted Orbital Transfer," *Journal of the Astronautical Sciences*, Vol. 38, No. 3, 1990, pp. 311–333.

[11]Guelman, M., "The Attainability Domain of a Coasting Vehicle," *Journal of Optimization Theory and Applications*, Vol. 39, No. 3, 1983, pp. 417–430.

[12]Grantham, W. J., and Vincent, T. L., "A Controllability Minimum Principle," *Journal of Optimization Theory and Applications*, Vol. 17, Nos. 1/2, 1975, pp. 93–114.